Biological response to hydrodynamic factors in estuarine-coastal systems: a numerical analysis in a micro-tidal bay.

Marta F-Pedrera Balsells [1]*, Manel Grifoll[1], Margarita Fernández-Tejedor[2], Manuel Espino[1], Marc Mestres[1], Agustín Sánchez-Arcilla[1].

[1] Maritime Engineering Laboratory (LIM), Catalonia University of Technology (UPC), 08034 Barcelona, Spain;
[2] Institute of Agriculture and Food Research and Technology (IRTA), Crtra. Poble Nou, s/n Km 5,5. 43540 Sant Carles de la Rapita, Spain;
* Correspondence: marta.balsells@upc.edu (M.F-P.B.)

Abstract:

Phytoplankton primary production in coastal bays and estuaries is influenced by multiple physical variables, such as wind, tides, freshwater inputs or light availability. In a short-term perspective these factors may influence the composition of biological variables such as phytoplankton biomass, as well as the amount of nutrients within the waterbody. Observations in Fangar Bay, a small, shallow, stratified and micro-tidal bay in the Ebro Delta (NW Mediterranean Sea), have shown that during wind episodes the biological variables undergo sudden variations in terms of concentration and distribution within the bay. The Regional Ocean Model System (ROMS) coupled with a nitrogen-based nutrient, phytoplankton, zooplankton, and detritus (NPZD) model has been applied to understand this spatio-temporal variability of phytoplankton biomass in Fangar Bay. Idealised simulations prove that during weak wind events ($< 6\ \mathrm{m\cdot s^{-1}}$), the stratification is maintained and therefore there is no dynamic connection between surface and bottom layers, penalizing phytoplankton growth in the whole water column. Conversely, during intense wind events ($> 10\ \mathrm{m\cdot s^{-1}}$) water column mixing occurs, homogenising the concentration of nutrients throughout the column, and increasing phytoplankton biomass in the bottom layers. In addition, shifts in the wind direction generate different phytoplankton biomass distributions within the bay, in accordance with the dispersion of the freshwater plumes from existing irrigation canals. Thus, the numerical results prove the influence of the freshwater plume evolution on the phytoplankton biomass distribution, which is consistent with remote sensing observations. The complexity of the wind-driven circulation due to the bathymetric characteristics and the modulation of the stratification implies that the phytoplankton biomass differs depending on the prevailing wind direction, leading to sharp Chl *a* gradients and complex patterns.

Keywords: phytoplankton biomass, ROMS-NPZD model, wind, biological parameters, physical parameters, Fangar Bay.

1. Introduction

The intense biological activity of estuaries and coastal bays and their importance as a source of resources and socio-economic services is well known. The influence of the terrestrial environment and human activity in these domains provides the nutrients necessary to create ecosystemic value (Lohrenz et al., 1997). The biological evolution of these waterbodies is strongly affected by physical factors. For instance, strong winds may control the inner water circulation (Geyer, 1997; Alekseenko et al., 2013; Cerralbo et al., 2015) and, together with topographic effects, can even cause the current to flow against the wind direction in the central channels (Xie & Li, 2018; F-Pedrera Balsells et al., 2020a). Freshwater inputs can also have a considerable effect on the water circulation (Cerralbo et al., 2014) and, acting as fluvial nutrient suppliers, can determine the temporal and spatial variability of phytoplankton biomass (de Madariaga, 1995; Geyer et al., 2018; Jiang et al., 2020). In this sense, the use of coupled physico-biological numerical models as a tool to understand the complexity of the phytoplankton regulatory mechanism in estuaries has increased in recent years, complementing *in situ* data and satellite imagery (Llebot et al., 2010; Artigas et al., 2014; Jiang et al., 2020). These numerical models can provide information on the current state of the estuary, create hypotheses and numerical experiments, and predict certain events and ecosystem responses (Stow et al., 2009; Llebot et al., 2010).

In small and shallow estuaries, the effects of both the physical mechanisms and biological behaviour become more complex due to the geometry of the basin itself. Moreover, in the bays of the Ebro Delta (i.e. Alfacs in the southern hemidelta and Fangar in the northern hemidelta), freshwater discharges from rice field irrigation channels also play an important role, together with aquifer contributions, being an important source of both organic and inorganic nutrients for coastal areas (Jou et al., 2019). In a small-scale coastal bay such as Fangar Bay, where depths are only of a few metres, chlorophyll a (Chl *a*) concentrations tend to show a high variability on a seasonal scale rather than on an interannual scale (Llebot et al. 2011), with higher concentrations found during the summer (Fernández and Galimany 2007). In this sense, Chl *a* concentrations in Fangar Bay tend to show a distinct seasonal fluctuations entailing larger variability in comparison as compared to other coastal domains such as the Ría de Arousa (Ramón et al., 2007) or Alfacs Bay (Artigas et al., 2014).

Previous investigations in Fangar Bay revealed that, during wind episodes, the biological variables undergo sudden variations in terms of concentration and distribution within the bay (F-Pedrera Balsells et al., 2021). Llebot et al. (2010) implemented a numerical model in Fangar Bay to determine the temporal distribution of phytoplankton and nutrients throughout the year. They determined that the highest concentration of phytoplankton occurred during the first months of the year with open irrigation channels, i.e., in the spring and early summer, but the role of episodic wind events remained unclear. F-Pedrera Balsells et al. (2021) investigated using observations the phytoplankton distribution resulting from different short-term wind episodes typical of the Ebro Delta area focusing on the summer months when substantial observations of bio-hydrodynamics where available. *In situ* measurements obtained during specific field campaigns and remote sensing observations suggested a link between the breaking of the stratification during these episodes and the Chl *a* distribution in the bay, with intense winds causing an increase in the Chl *a* concentration values. The role of the discharges from the irrigation channels remained unclear because the freshwater outflow was constant during the field campaigns. Also, the spatio-temporal variability of the Chl *a* concentration observed in the field campaigns was quite complex due to the many factors involved, and deserved additional modelling efforts. In consequence, the objective of this contribution is to investigate the biological response of the bay to wind episodes and freshwater inputs through the combination of idealised numerical simulations and observations. For this, a biogeochemical model is coupled into a validated hydrodynamic model to reproduce the dynamics within the bay and provide answers to unresolved questions suggested by F-Pedrera Balsells et al. (2021) and Llebot et al. (2010) in terms of spatial and temporal variability on Chl *a* in shallow and coastal bays. Extensive field data and previous hydrodynamic knowledge converts Fangar Bay in a unique study area to investigate the biological response in an area with large spatio-temporal variability in Chl *a* evolution.

2. Material and Methods

2.1. Study area

Fangar Bay is part of the Ebro Delta (NW Mediterranean Sea), which forms two semi-enclosed bays, Fangar to the north and Alfacs to the south. Of these, Fangar Bay is the smallest, extending over 12 km^2, with a length of about 6 km, a maximum width of 2 km and a volume of water of $16\cdot10^6$ m^3 (Delgado and Camp 1987). The average depth is 2 m, with a maximum of 4 m (see bathymetry in Figure 1). Its connection with the open sea is oriented to the NW, and is approximately 1 km wide (Garcia and Ballester 1984), although it is currently narrowing because of the accumulation of sediment from the beach located to the north (Archetti, Bernia, and Salvà-Catarineu 2010).

The wind regime in the Fangar Bay area is characterized by the presence of S/SE sea breezes – which do not exceed 6 m$\cdot$s^{-1} during spring and summer– and strong winds from the N and NW of more than 12 m$\cdot$s^{-1} in autumn and winter (Bolaños et al. 2009; Grifoll et al. 2016). The most frequent wind throughout the year is locally known as Mestral, which is characterized by strong gusts of cold and dry wind from the NW (Garcia and Ballester 1984). These winds are associated to the general weather pattern and occur throughout the year, but show maximal strength and persistence during the colder months. Additionally, E and SE winds that can also be quite intense (~10 m$\cdot$s^{-1}) are responsible for local rain events and transient increases of the local mean sea level at the coast (Muñoz 1990).

Both the Ebro Delta bays receive freshwater inputs from the channels irrigating the Delta paddies. This freshwater outflow is regulated by the rice cultivation cycle throughout the year. In Fangar Bay, the channels are open between April and November, discharging a mean flow of 7.23 $m^3 \cdot s^{-1}$ (*SAICA Project, 2013. Available online: https://www.saica.co.za/ (accessed on 30 January 2020)*), whereas the outflow is negligible from December to March, when the channels are closed (Perez & Camp, 1986). There are two main freshwater discharges in Fangar Bay: one in the Illa de Mar harbour inside the bay (IM in Figure 1) and the other one, Bassa de les Olles, located at the bay mouth (BO in Figure 1). In addition to these, freshwater inputs are also expected inside the bay from groundwater sources (Camp and Delgado 1987), and along the coastline where freshwater inflows regulated by gravity according to the sea level occur. In both cases, the expected freshwater inflow is smaller than that discharged from the regulated irrigation channels.

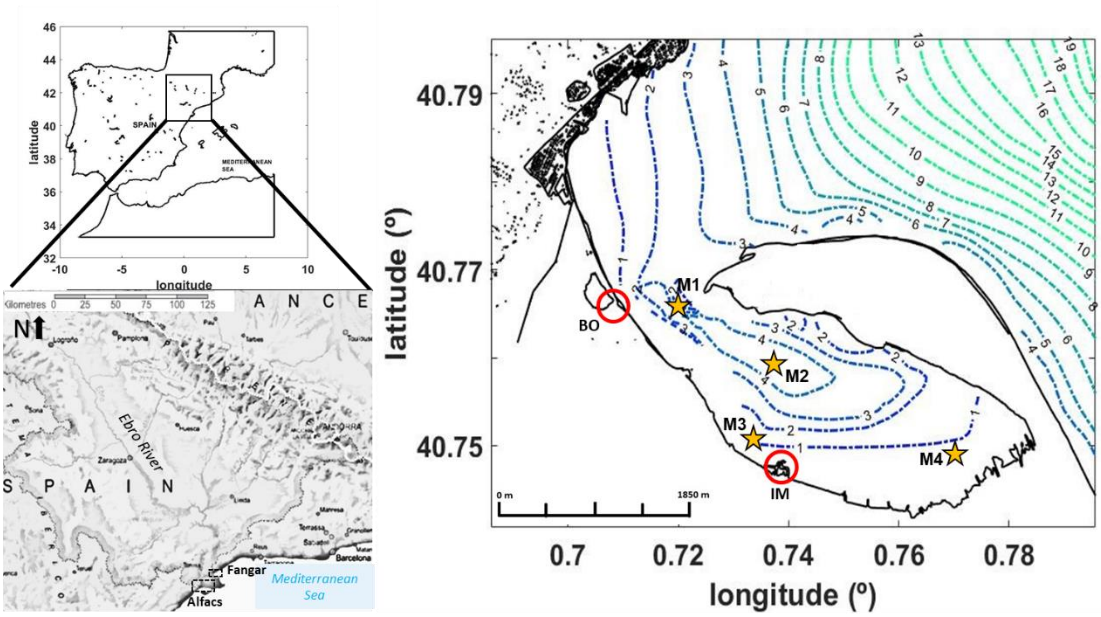

Figure 1. Location of the study area. The red circles show the two main points of freshwater discharges (Bassa de les Olles (BO) and Illa de Mar (IM). The yellow stars show the location of the control points used for the numerical model results (Table 1). The bathymetry is also shown in the figure.

Fangar Bay is micro tidal, with a tidal range smaller than 1 m, which accentuates the action of the wind, and is stratified most of the year mainly due to the freshwater flows rather than to the atmospheric heat fluxes. Because of its bathymetry and complex geometry there is a strong transverse variability of the water flows, particularly for prevalent up-bay wind episodes (NW winds), during which up-bay flow occurs in the lateral shoals and down-bay flow in the central channel for up-bay wind pulses. These winds also cause homogenisation of the whole water column. On the other hand, during calm periods the water circulation is complex: current velocities are very small and lack a clear pattern, and the bay is strongly stratified due to the freshwater inputs from the drainage channels (F-Pedrera Balsells et al., 2020a).

Table 1. Location of control points and drainage channels mouths

	Latitude (º)	Longitude (º)	Depth (in m)
M1	40.775306	0.720305	4.05
M2	40.767762	0.742785	4.02
M3	40.771534	0.735841	1.79

M4	40.758125	0.771917	0.93
BO	40.785970	0.709483	-
IM	40.766413	0.738546	-

2.2. Numerical model and experiments design

To analyse the relationship between the hydrodynamic and Chl *a* response to wind in small and shallow estuaries, the Regional Ocean Modelling System (ROMS) was used to perform a series of numerical experiments. The ROMS numerical model is a 3D, free-surface, terrain-following numerical model that solves the Reynolds-Averaged Navier-Stokes equations using hydrostatic and Boussinesq assumptions (Shchepetkin and McWilliams 2005). To discretize the horizontal grid into curvilinear orthogonal coordinates and finite difference approximations on stretched vertical coordinates, ROMS uses the Arakawa-C differentiation scheme (Haidvogel et al. 2007). The numerical details of ROMS are described extensively in (Shchepetkin and McWilliams 2005). This model has been used and validated in similar bays and estuaries, such as Alfacs Bay located south of the Ebro Delta (e.g. Cerralbo et al., 2014, 2015, 2019) and in the Fangar Bay (see Appendix 1). The domain used for the experiments consists of a regular 107x147 grid with a horizontal resolution of about 70 m and 10 sigma levels in the vertical direction (F-Pedrera Balsells et al. 2020a). The model boundary is located 10 nodes away from the bay's entrance to avoid boundary noise. The hydrodynamic bottom boundary layer was parametrised with a logarithmic profile using a characteristic bottom roughness height of 0.2 m. The turbulence closure scheme for the vertical mixing was the generic length scale (GLS) tuned to behave as a k-ε (Warner et al., 2005). Horizontal harmonic mixing of momentum was defined with constant values of 5 $m^2 \cdot s^{-1}$.

The NPZD numerical model coupled with the ROMS model includes dissolved inorganic nitrogen, phytoplankton, zooplankton and detritus (Franks 2002). The initial nitrate concentration was taken from field data collected by IRTA between the years 2009-2012 (ACA, 2012), and the initial phytoplankton concentrations were collected from observation data during the year 2019, whereas the initial zooplankton concentration was estimated from the literature (Rico 2015; Powell et al. 2006). The units in which these data were collected were $mg \cdot m^{-3}$. The NPZD model uses $mmol \cdot m^{-3}$ units, so a conversion has been made using the mole fraction of Chl *a* (893.51 $g \cdot mol^{-1}$) (see Table 2). The rest of input variables for the ROMS-NPZD model were acquired from Llebot et al. (2010), and are detailed in Appendix B (Table B1), together with the model equations. Short-term simulations (5 days each) were carried out to analyse the response of biological variables to the wind. This simulation length exemplifies the typical wind events in the area, lasting from 3 to 5 days (except the daily sea breeze during spring and summer) (Ràfols et al. 2017). Six experiments were designed with varying wind intensity and direction, and varying freshwater input from channels. The wind parameters are based on wind measurements in the Fangar area (F-Pedrera Balsells et al., 2020a), with weaker down-bay winds (associated to daily sea breeze, DW6 simulation), SE down-bay winds (DW8 simulation), NW up-bay winds (UW10 simulation) and strong NW up-bay winds (UW12 simulation) and in addition to a simulation where the flow out of the drainage channels was reduced by half (UW12fr). For theoretical comparison, a simulation was also carried out with 0 $m \cdot s^{-1}$ wind intensity (CALM simulation). All simulations are summarized in Table 2. Temperature and salinity conditions were in accordance with those measured within the bay (see field campaign description in F-Pedrera Balsells et al., 2021). In addition, Figure 3 shows the horizontal distribution of modelled salinity based on initial conditions interpolated from the observation shown in F-Pedrera Balsells et al. (2021). Freshwater contributions were activated to monitor the evolution of nutrient inputs from the irrigation channels. Both channels (BO and IM, Figure 1) provide nutrients that will be presumably dispersed within the bay due to the combined action of currents and wind.

Table 2. Summary of the idealized numerical simulations using the ROMS-NPZD model for Fangar Bay.

Simulation	Wind direction	Intensity wind ($m \cdot s^{-1}$)	Channel flow ($m^3 \cdot s^{-1}$ each channel)	Initial nitrate concentration ($mmol \cdot m^{-3}$)	Initial phytoplankton biomass ($mmol \cdot m^{-3}$)	Initial zooplankton biomass ($mmol \cdot m^{-3}$)
CALM	-	0	7.5	2.73	0.27	0.08
DW6	Down-bay wind	6	7.5	2.73	0.27	0.08
UW10	Up-bay wind	10	7.5	2.73	0.27	0.08
DW8	Down-bay wind	8	7.5	2.73	0.27	0.08
UW12	Up-bay wind	12	7.5	2.73	0.27	0.08
UW12fr	Up-bay wind	12	3.75	2.73	0.27	0.08

2.3. Satellite image processing

To qualitatively compare the numerical modelling results with real observations, satellite images from Sentinel-2, level 1-C, are used. These satellites carry a single optical instrument, the MultiSpectral Imager (MSI), and its swath width (290 km) and high revisit time (10 days at the equator with one satellite and 2–3 days at mid-latitudes) support monitoring of Earth's surface changes. Chlorophyll-*a* concentrations were computed automatically by the Sentinel Application Platform (SNAP) (https://step.esa.int/main/toolboxes/snap/, accessed on 25 February 2021). The MSI sensor has had an atmospheric correction applied to it with a C2RCC processor (Case 2 Regional CoastColour, Brockmann et al., 2016) to obtain the Chl *a* images. The images correspond to remote sensing obtained after intense wind episodes (see details in F-Pedrera Balsells et al., 2021).

3. Results

Four points within the bay were chosen to investigate the temporal evolution of the biological variables obtained from the NPZD model: in the mouth area (M1), in the centre of the bay (M2), in a coastal area in front of the IM discharge point (M3) and in the innermost part of the bay (M4) (Figure 1, Table 1). Both channels (BO and IM, Figure 1) provide nutrients which increase the concentration of phytoplankton biomass within the bay. Figure 2 shows the time series of the numerical simulation in terms of nitrates and phytoplankton at the four control points. The nitrate concentration tends to decrease gently during the simulation, consistent with the increase in phytoplankton biomass and zooplankton. Stratification conditions (CALM and DW6 simulations) show higher phytoplankton biomass concentrations at the surface due to freshwater fluxes. Substantial differences of phytoplankton biomass between surface and bottom layers are evident in M1, where the stratification tends to be stronger in contrast to the shallowest point (M4). The inner point M4 also shows a clear correlation of the wind intensity and the phytoplankton biomass values: as the up-bay wind intensity increases (i.e. UW12, larger than UW10) the phytoplankton biomass also increases. In all cases the numerical simulations suggest large temporal and spatial variability within the bay.

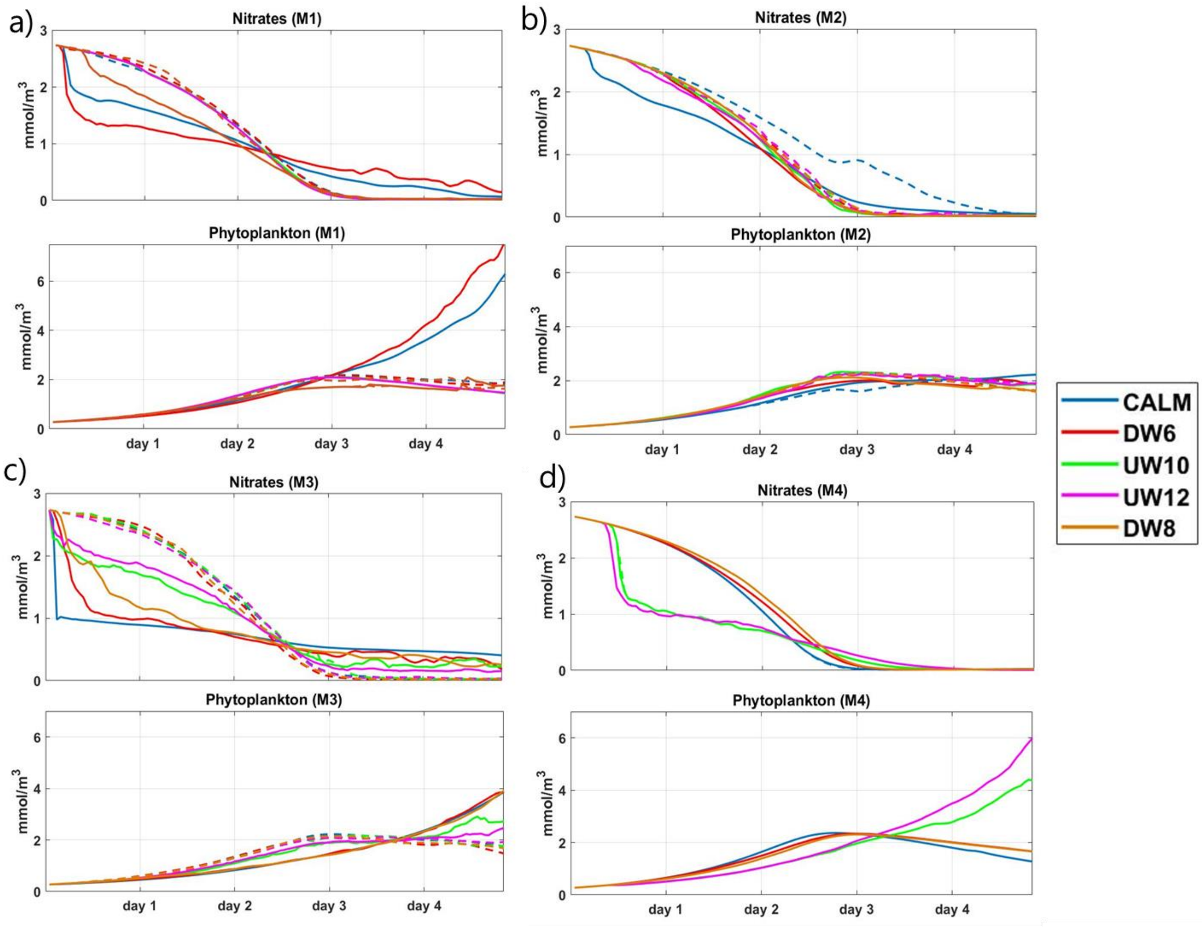

Figure 2. Time series of the nitrates and phytoplankton biomass at different points of the bay: (a) M1, (b) M2, (c) M3 and (d) M4. The different colours show the different simulations with in function of the wind. Solid lines show the numerical results at the sea surface, dashed line shows numerical results at the sea bottom.

Intense wind was associated to the homogenisation of the initially stratified water column. In particular, for the UW10 and UW12 simulations (moderate and strong up-bay wind), both surface and bottom phytoplankton time series coincide at all control points. Differences in growth rates between phytoplankton and zooplankton biomass are observed in the time series. While phytoplankton can multiply rapidly under favourable concentrations of light and nutrients, increases in zooplankton numbers often lag considerably behind due to their slower generation times. Consequently, when phytoplankton biomass peaks and nutrients decline, zooplankton biomass may remain low as they begin to grow in response to the high food supply (data not shown). These relations are consistent with the diagram shown in the Appendix B (Figure B1).

In order to examine the spatial variability, Figure a shows the differences in phytoplankton biomass at the end of the simulation in comparison to the initial concentration values. Surface and bottom values are displayed according to the terrain-following sigma coordinates of the numerical model. All the simulations present positive values, indicating an increase of phytoplankton biomass due to the nutrients provided by the freshwater input. During up-bay winds (simulations UW12 and UW12fr), the phytoplankton biomass increases in the inner zone, both at the surface and at the bottom, with concentrations larger than 5 mmol·m^{-3}. This coincides with vertical mixing of the water column, as shown by the salinity distributions (Figure 3b). In contrast, during no wind and weak (CALM and DW6) winds, the highest phytoplankton biomass (4 mmol·m^{-3}) is located in front of the discharge points, with the largest values obtained at the point inside the bay (M3, 10 mmol·m^{-3} at the surface). For no wind simulation (CALM simulation) stratified conditions remain. In this case, bottom concentrations are small (1 mmol·m^{-3}) in comparison to other cases, highlighting the positive effect of strong winds on the vertical distribution of phytoplankton biomass. During the DW8 simulation, the highest concentrations are also observed near the discharge points (M1 and M3), with the highest values found towards the mouth, consistent with the presence of a low-salinity plume. Overall, there is a correspondence between the freshwater plume and the phytoplankton biomass. Therefore, the wind-driven evolution of the plume has a very important impact on the final distribution of Chl *a*. In the same way, it can be seen in Figure 3a that winds of similar intensities but different directions (DW8 vs. UW12) lead to very different results in terms of the horizontal distribution of phytoplankton biomass. Finally, the results of an additional simulation similar to UW12 but with half the channels outflow rates (UW12fr) revealed a horizontal distribution similar to UW12, but with smaller phytoplankton biomass concentrations associated to the lower nutrient input.

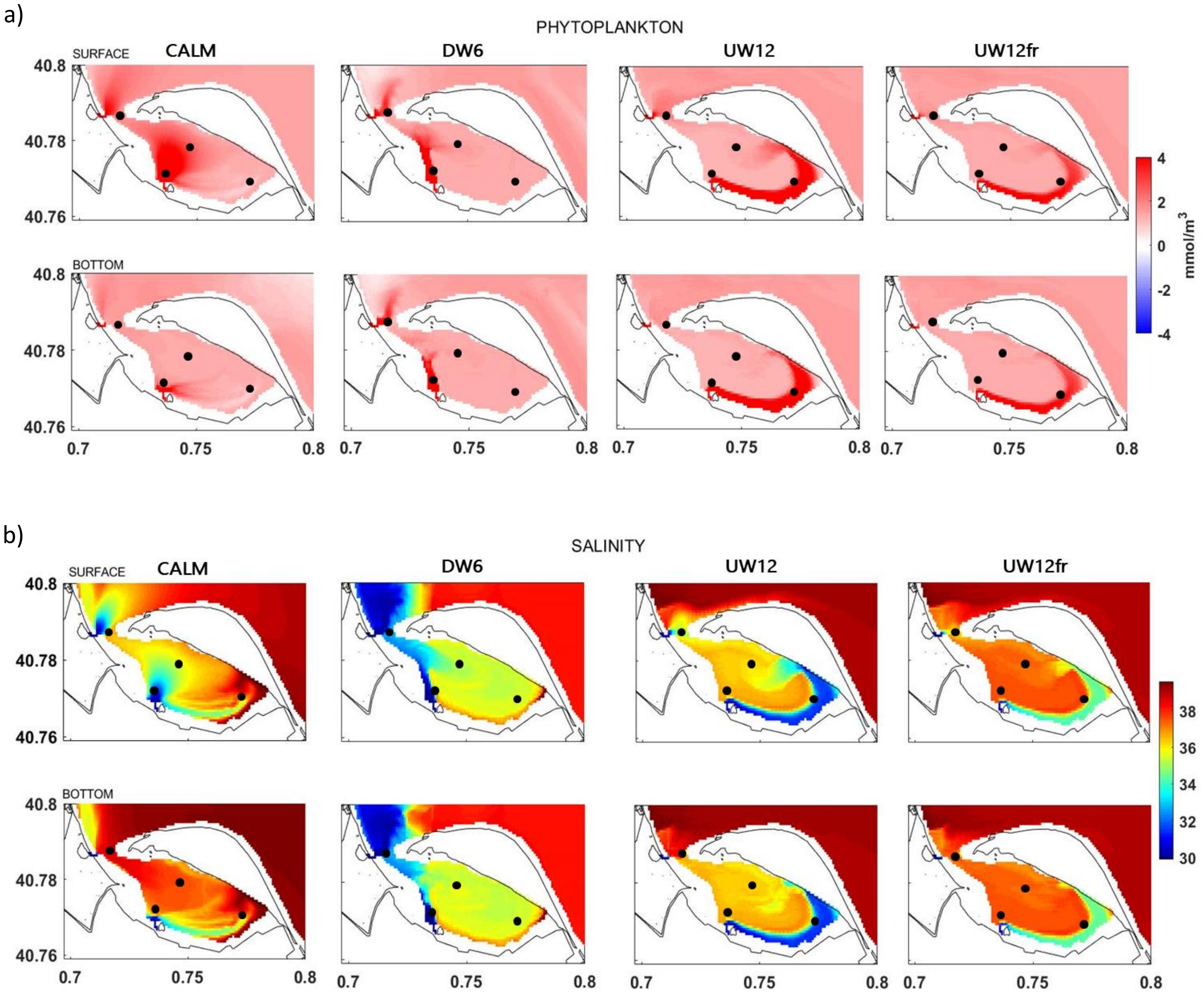

Figure 3. Differences in phytoplankton biomass (surface and bottom) at the end of the simulation in comparison to the initial concentration values (a) and surface and bottom salinity (b) according to different numerical simulations. The numerical control points are also marked with black dots.

Differences in the distribution of phytoplankton biomass, nutrient concentration and salinity are also observed in Figure 4. It shows the vertical profiles after a three-days simulation at the four points mentioned above for the DW6 (weak down-bay wind), DW8 (SE down-bay wind) and UW12 (NW up-bay wind) simulations. These profiles show homogeneous concentrations of phytoplankton biomass and salinity in the water column after strong wind episodes (DW8 and UW12). In contrast, during weaker winds (DW6) the saline stratification tends to remain in M1 and M3, leading to a larger presence of phytoplankton biomass in the surface layers. At the innermost point of the bay (i.e., M4), the phytoplankton biomass is homogeneous in all simulations since, due to the shallowness of the area (less than 1 m deep), even weaker winds are able to mix the water column. During calm winds, the highest biomass value is found in front of the freshwater discharge points (M1 and M3). During strong NW up-bay winds (UW12), the highest biomass values are found in the innermost area of the bay (M4), while during strong SE down-bay winds (DW8) the largest biomass concentration is observed at the coastal point inside the bay (i.e., M3), with higher values than during the UW12 simulation. The comparison of profiles at M3 shows a high variability of phytoplankton biomass values: DW8 shows larger values of phytoplankton biomass as compared to DW6. This means that the mixing mechanism can favour the increase of phytoplankton biomass. Finally, the similarity in M3 between DW8 and UW12 also suggests the effect of the freshwater plume on the phytoplankton biomass, which will be discussed later. As it can be seen in Figure 4c, there is nutrient input at the initial moment (continuous lines) and then there is a consumption by phytoplankton that reduces this concentration (dashed lines). With this simple model, where there is no further contribution of nutrients neither by the suspended sediment nor by the input from the open sea they are almost depleted by the end of the simulation.

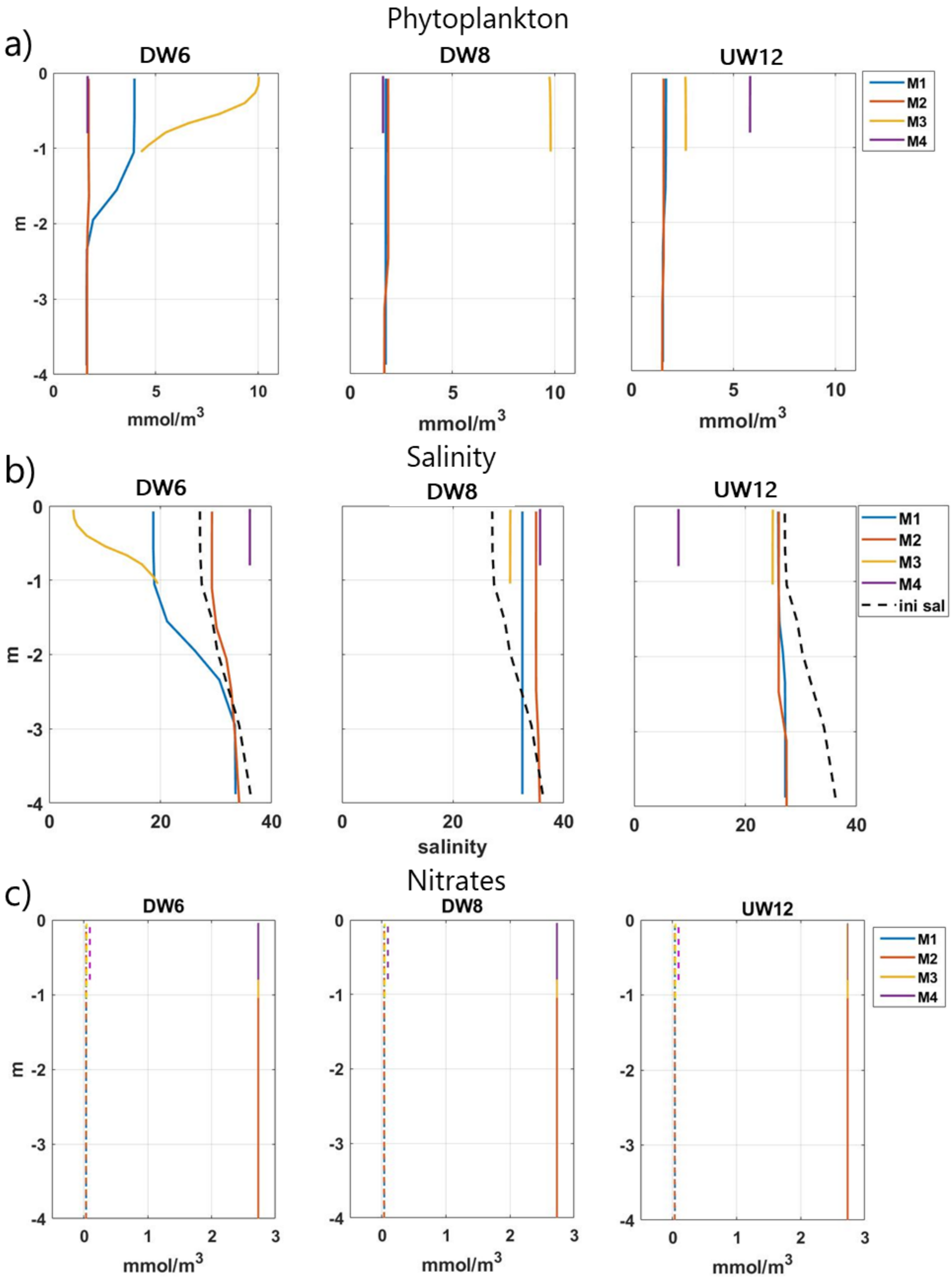

Figure 4. Phytoplankton biomass (a), vertical salinity profiles (b) and nitrates concentration (c) as a function of wind events simulations at the four sampling points: M1 (blue), M2 (orange), M3 (yellow) and M4 (purple). Dashed black line shows the initial salinity. For nitrates, the solid lines show the initial concentrations and the dashed lines show the final concentrations.

A qualitative comparison of the idealised coupled simulations with *in situ* data and remote sensing provides robustness to our analysis. The increase of phytoplankton in the first days of the numerical simulations (see Figure 4) are consistent with the conclusions drawn by F-Pedrera Balsells et al. (2021) which pointed out that wind episodes cause an increase in the concentration of surface Chl *a*. Chlorophyll *a* field data were obtained using seawater samples (F-Pedrera Balsells et al. 2021) and the range obtained after wind events were 4 $mg \cdot m^{-3}$ and 7 $mg \cdot m^{-3}$. These values agree with the values obtained after 5 days of wind simulations (e.g. ~5 $mmol \cdot m^{-3}$) assuming a 1.59 g chlorophyll per mole N conversion suggested by Gong et al. (2015) (Cloern & Nichols 1985; Fasham et al., 1990; Oschlies 2001). Maximum reported concentration of Chl *a* measured in Fangar Bay has been 25 $mg \cdot m^{-3}$ in September 1983 at 4 m depth (Delgado 1987) and 11 $mg \cdot m^{-3}$ in October 2005 (Quijano-Scheggia et al. 2008). Also, vertical variability of Chl *a* of the order of 5 $mg \cdot m^{-3}$ has been measured within the bay, suggesting the influence of the forcing mechanism and its interaction with primary production. Figure 5 shows a similarity between the model results and the Sentinel-2 satellite images, in periods of calm or weak wind, and strong wind which produces mixing (NW up-bay wind). The satellite images correspond to 15 July 2019 (Figure 5d) and 11 August 2019 (Figure 5c), one day after an up-bay wind episode occurred on 14 July 2019, and during a sea-breeze period (weak winds) between 30 July and 12 August 2019, respectively. Note that the satellite image of the up-bay wind episode is from a few days after the wind has blown, while the model results correspond to the effects of a steady wind. In spite of this, there is an identifiable correlation between model and images. For calm or weak down-bay wind (sea breeze), the phytoplankton biomass is relatively low, only present in the areas close to the discharge channels following the coastline consistent with the wind-driven currents due to sea breeze. During NW up-bay winds, phytoplankton biomass increases in the inner zone and is later dispersed within the bay. In any case, it should also be taken into account that the satellite, being such a shallow area, does not only show data on phytoplankton chlorophyll but also on macrophytes, which are very present in this bay (Soriano-González et al. 2019).

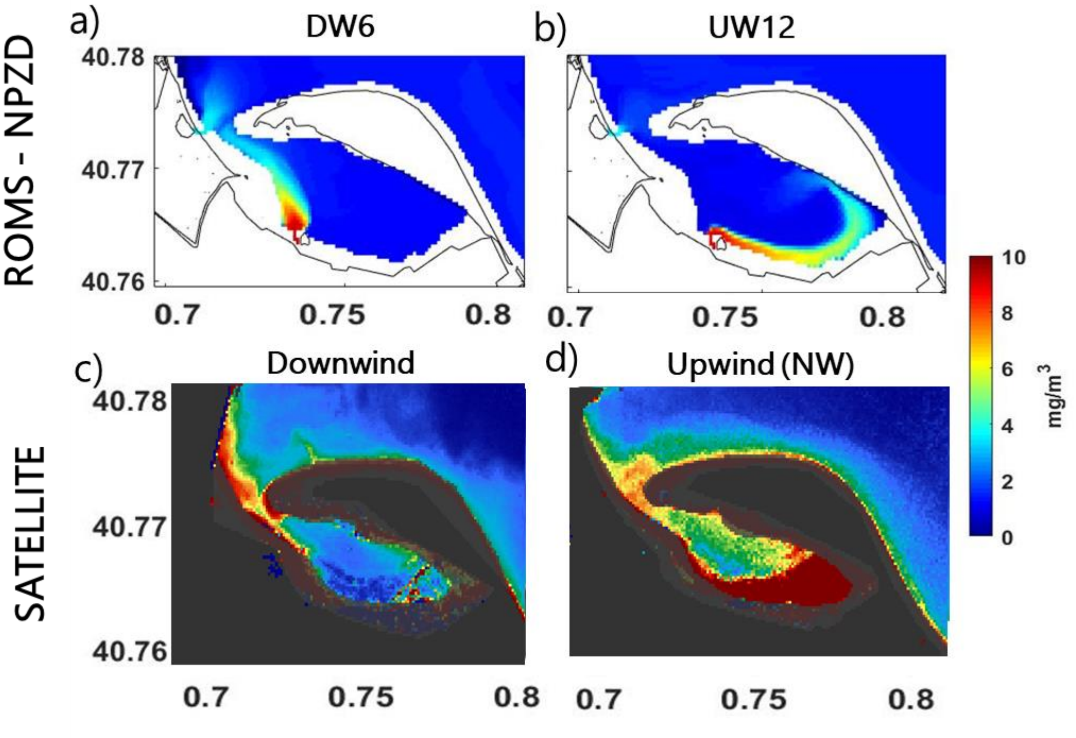

Figure 5. Similarity of surface model results with Sentinel 2 satellite images. (a) and (b) show model results during breezes and strong NW winds, respectively. (c) and (d) show corresponding satellite images with the same wind episodes.

4. Discussion

The phytoplankton distribution is controlled by turbulent mixing and advection factors, which are affected by physical forcings such as wind, tides and continental freshwater and nutrient input. In tidallydominated estuaries or upwelling areas, phytoplankton biomass is distributed according to spring blooms, where algal blooms generated during upwelling events are transported to the bays through various physical mechanisms (tidal stirring, and gravitational and wind-driven circulation (Hickey and Banas, 2003; Martin et al., 2007), as occurs in the Eastern Scheldt Bay (Jiang et al. 2020) or the Rías Baixas of Galicia (Reguera et al., 1993). On the other hand, in estuaries where the tide is practically non-existent and the depth is small, phytoplankton growth is limited by nutrients and the turbidity of the water due to large inputs of sediment from rivers and channels, such as in the Chilika lagoon (Srichandan et al., 2015) or our study area, the Fangar Bay.

From a hydrodynamic point of view, Fangar Bay is complex due to its intricate bathymetry and shallowness which suggest a fast wind-driven response (Llebot, 2010; F-Pedrera Balsells et al., 2020a). The numerical results have proved that the wind affects the direction and magnitude of surface currents, disperses or reinforces fronts, and induces vertical mixing, in accordance with other investigations (Geyer, 1997; Llebot et al., 2014; F-Pedrera Balsells et al., 2020a). The distribution of phytoplankton biomass in Fangar Bay agrees with water currents driven by the local winds (current magnitude 0.1 $m \cdot s^{-1}$) and modulated by the complex bathymetry of the basin (F-Pedrera Balsells et al., 2020a) and the evolution of the freshwater plume of the drainage channels (Figure 3b). The complexity of the hydrodynamic and biological variables suggests to face the analysis using “idealized” or “simplified” conditions instead of realistic (and long-term) simulations. We proved that these short simulations (of the order of the wind duration events) have been useful to understand the main hydro-biological coupled processes. It is true that more than 5 days would be required to simulate the evolution of the biological variables, but we wanted to adjust the simulations to the duration of the wind events observed in the region (Ràfols et al. 2017), to explore the response to this phenomenon (i.e. short-term response). This wind duration seems to be too short, but in order to understand the fundamental processes and the link of biological and hydrodynamic variables this duration was enough. Results of larger simulations have been also analysed (not shown) but those become unfeasible according to the observations of primary production.

The model results have shown the combined effect of the wind on phytoplankton biomass distribution within the bay from two perspectives. On the one hand, intense wind episodes are able to break the stratification, mixing the water column and leading to an increase of phytoplankton biomass in the deeper levels of the bay. Simulations with no wind (CALM), in which the bay remains stratified, are characterized by the presence of a physical barrier that prevents nutrient vertical transfer, so the phytoplankton biomass remains in the surface layers. This case shows how the absence of wind (or even the presence of sea breezes) causes the phytoplankton biomass dispersion to be governed by the estuarine circulation of the bay, with phytoplankton biomass decreasing in the seaward direction. A similar seaward negative gradient of phytoplankton is found in other estuaries and coastal systems in which the nutrient gradients control the phytoplankton distribution (Soetaert et al., 2006; Gomez et al., 2018). When strong NW up-bay winds blow in Fangar Bay, the water column homogenises, making nutrients available throughout the water column, both at the surface and at the bottom (i.e., UW10 and UW12 simulations). The phytoplankton biomass is advected towards the inner part of the bay, following the water currents induced by the NW winds, not only at the surface but throughout the water column. With strong SE down-bay winds (DW8 simulation), phytoplankton biomass increases near the discharge channels and the phytoplankton biomass distribution follows the water circulation driven by SE winds: seaward flow in the lateral shoals (F-Pedrera Balsells et al., 2020a). Figure 6 summarize the main processes discussed above. The strong winds episodes suggest a non-uniform distribution of phytoplankton biomass with irregular patterns and patches attributed to a dominant source factor (see examples in Ahel et al., 1996; Geyer et al., 2018; Jiang et al., 2020), which in the case of Fangar Bay is a role played by the discharge channels. In consequence, following the categorization exposed by Jiang et al. (2020) in terms of spatial patterns of phytoplankton biomass in estuaries and coastal bays, Fangar Bay may be included in different typologies depending on the wind configuration from a short-term perspective.

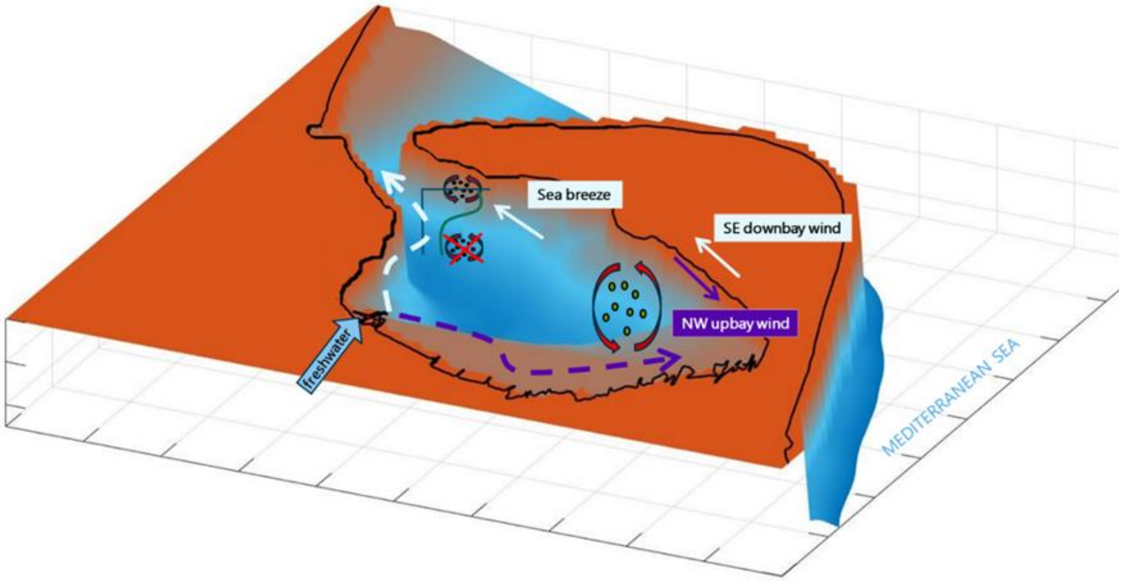

Figure 6. Conceptual diagram of estuarine processes affecting phytoplankton distribution in Fangar Bay. Strong NW up-bay winds cause mixing of the water column and the freshwater plume to move inland. Strong SE down-bay winds also cause mixing, but the freshwater plume moves seaward. Sea breezes also cause a seaward displacement of the freshwater plume, but does not break the vertical stratification, so there is a difference between phytoplankton biomass at the surface and at the bottom.

The second effect of the wind is related to the wind-driven plume dispersion. Freshwater discharges from the irrigation channels are the dominant drivers of salinity and nutrient gradients. In Fangar Bay there is a co-limitation of nitrogen and phosphorus, with the most limiting nutrient changing throughout the year, depending on the variability of sources and sinks of both nutrients (Llebot et al. 2010). The NPZD model considers nitrogen only and assumes no phosphorus limitation in phytoplankton growth. This sets a limit on the full understanding of Fangar Bay's dynamics, but our analysis provides a first interpretation of the data. Freshwater discharges also vary over the year, depending on whether these irrigation channels are closed (January to March), open (April to November) or semi-open (November and December). In F-Pedrera Balsells et al. (2021) it was observed that after strong NW up-bay wind episodes, phytoplankton biomass tended to increase within the bay, but it could not be determined whether this behaviour extended to the entire water column as the simulations presented herein suggest. As described in other works (Simpson & Bowers, 1981; Horsburgh et al., 2000) vertical density stratification is an important determinant of ecosystem characteristics.

Ultimately, in a small, shallow, micro-tidal bay, the wind generates very complex currents and causes large spatial and temporal variability in the distribution of phytoplankton biomass. Chl *a* peaks usually form at the front of the river plume, either by rapid nutrient assimilation and growth or by aggregation along the strong salinity gradient of this transition (Geyer et al., 2018). This explains why the highest biomass levels can be found following the river plume, as shown in Figure 3. Therefore, the same simulations were performed by halving the channel outflow and the results on phytoplankton biomass distribution were the same, only lower, due to lower nutrient input. Some studies have shown that Chl *a* concentration is higher in the freshwater areas of the bay and decreases as salinity increases. This leads to high phytoplankton biomass in the plume formed by freshwater tributaries, which discharge high levels of nutrients, as can happen in the Scheldt River and Western Scheldt Estuary in Belgium (Soetaert et al., 2006).

Freshwater discharges from irrigation channels also control water residence times within the bay. Prolonged residence times generally facilitate the growth and accumulation of phytoplankton biomass (Wan et al. 2013). The location and magnitude of phytoplankton biomass can be partly explained by residence time, although phytoplankton productivity may be affected by other factors such as nutrient availability, light, temperature and zooplankton grazing (Wan et al. 2013). In Fangar Bay, residence time is in the range of about 20 days in the middle zone and about 40 days in the innermost quasi-stagnant zone (F-Pedrera Balsells et al., 2020b). This work also shows that an increase in freshwater discharge through the inner channel (IM) helps to decrease the residence time in the innermost zone (F-Pedrera Balsells et al., 2020b).

In turn, therefore, a reduction in river discharge increases residence time and may allow a higher concentration of phytoplankton to accumulate within the estuary. Our results show a higher concentration of phytoplankton biomass in the innermost zone consistent with the larger residence time.

Hydro-ecological coupled models can be useful in the characterization of the evolution and prediction of nutrient variables as a tool of aquaculture management. Cerralbo et al. (2019) suggest the need to implement numerical tools in Ebro delta bays for early warning systems to prevent eventual mussel mortality during summer. Moreover, it is possible to combine this type of models, where the biogeochemistry of the bay is analyzed together with the hydrodynamics, with simpler models such as those of carrying capacity (Weitzman and Filgueira 2020; Guyondet et al., 2022) for better aquaculture management including harvest planning and early warning systems to avoid mortality (Hargreaves 1998; Yu and Gan 2021). They can even be extended to socio-economic study models of the area to cover all aspects related to aquaculture activity. Also, the use of hydrodynamic and biogeochemical models supports Nature Based Solutions (NBS) as an alternative to traditional engineering, with growing relevance to design integrated solutions for building coastal bay resilience (Pontee et al.,2016; F-Pedrera Balsells et al. 2020b) under climate change. Initial set of environmentally adapted alternatives in Fangar Bay are: i) self-regulating connection with the open sea, ii) adjustable connection with land discharges or iii) adaptive reallocation of aquaculture activities; whose will require specific investigations on the hydro-biogeochemical response.

5. Conclusions and future works

Results based on remote observations and numerical models conclude that the biological variables in small-scale, shallow and micro-tidal bays (such as Fangar Bay) show strong gradients due to the influence of the wind and the freshwater plume evolution. Strong winds have a double impact: i) breaking down the stratification and mixing the water column, leading to an increase of phytoplankton biomass at the bottom, and ii) distributing the canal-borne nutrients within the bay, resulting in an irregular pattern of phytoplankton biomass. Due to the predominance of the wind forcing on the bay's water circulation, different wind directions and/or intensities may have a completely different effect on phytoplankton biomass distribution. In this sense, wind variability explains the complex pattern of phytoplankton biomass observed in the *in situ* measurements and remote sensing, characterized by sharp horizontal gradients. In particular, the link between the hydrodynamics and the phytoplankton evolution in Fangar Bay can be summarized as shown in Figure 6. This figure is a conceptual diagram of the estuarine processes affecting phytoplankton biomass distribution in a small-scale, micro-tidal bay. The distribution of these nutrients is further influenced by the surface currents induced by the different winds in the area. With weak down-bay winds (i.e. sea-breeze), stratification is maintained within the estuary, so higher phytoplankton biomass near the discharge points and at the surface layer are found. During strong up-bay and down-bay winds (i.e. North-westerlies, and South-easterlies, respectively), the stratification is broken, so the nutrients discharged from the channels are distributed homogeneously throughout the water column, facilitating phytoplankton growth in the deeper layers. This growth expands horizontally according to the wind-driven currents: towards the inner zone through the lateral shoals, in the case of up-bay winds, or towards the mouth zone, in the case of down-bay winds.

Fangar Bay is complex from both a hydrodynamic and biological standpoint. Different phytoplankton patterns are identified depending on the meteorological conditions and, to account for this, different idealised simulations were designed in order to approach each scenario separately. Even so, there are processes that remain unexplored such as the resuspension of Chl *a* containing biomass, the effect of long-duration wind episodes, the increase of freshwater flows due to heavy rain events, as well as the change in limiting nutrients that often occurs in such environments, affecting phytoplankton biomass, composition and seasonal cycling (D'Elia et al., 1986; Fisher et al., 1992; Grifoll et al. 2019). The sediment resuspension and increase of turbidity associated with wind events and other forcing mechanisms has been observed previously in Fangar Bay and similar domains (Grifoll et al. 2019; F-Pedrera Balsells et al. 2021). The incorporation of a sediment transport module to the numerical suite may provide information on the incorporation of biomass in the water column and the consequent increase of phytoplankton. The availability of N or P inside the bay also influences the biochemical composition of phytoplankton (Estrada et al., 2008). These topics remain to be studied in future work, as does the analysis of the impact of these dynamics on zooplankton and detritus, which are two variables also taken into account by the ROMS-NPZD model. This will lead to robust results for future realistic simulations (i.e. long-term) including hydrodynamic and biological coupled processes. In any case, the combined analysis of observations and numerical models has provided compelling results and opens new perspectives to understand the short term dynamics of shallow and micro-tidal bays to meteorological events from a combined hydro-biological point of view.

6. **Appendix A.** Model validation.

The numerical implementation in Fangar Bay consists of a telescopic three-grid two-way nested ROMS scheme, with a finer bay grid (resolution of about 70 m) embedded within a cascade of coarser grids (see Figure A1). The model has been validated by comparing modelled surface velocities from the coastal domain (~ 350 m) with data from the Ebro Delta High Frequency Radar (HFR, Lorente et al., 2015 at a random position, and modelled currents from the finest domain (~ 70 m) with vertical current profiles measured inside Fangar Bay during an October-November, 2017 field campaign. The observational data were, amongst others, current velocity and direction obtained every 10 min in 25 cm thick layers distributed from the bottom to the surface.

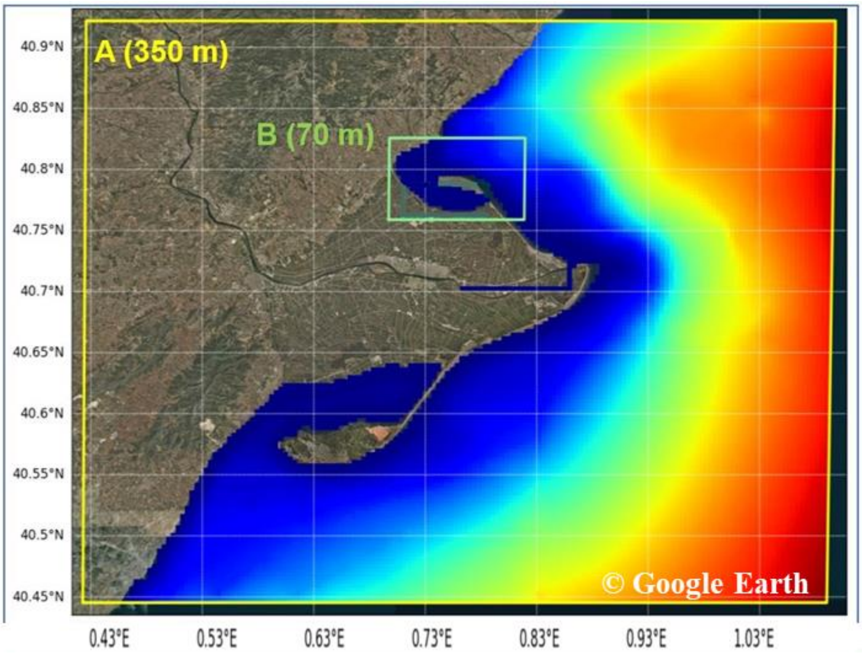

Figure A1. Ebro Delta and the Fangar Bay, with the telescoping domains used in the system. Conditions for ROMS at the A domain are obtained either from CMEMS-IBI or CMEMS-MED. Map from Google Earth (Data SIO, NOAA, U. S. Navy, NGA, GEBCO, Image Landsat/Copernicus © 2018 Google.

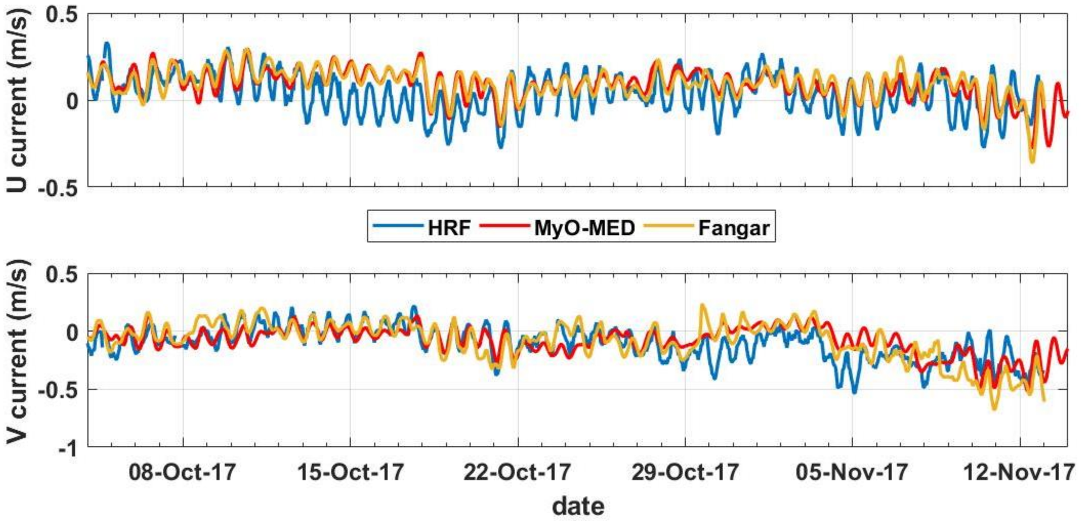

Figure A2. Surface zonal (U) and meridional (V) current components measured by the HRF radar (blue line) and modelled my CMEMS-MED (red) and the Fangar nested suite (yellow) off the Ebro Delta for domain A (350 m horizontal resolution grid).

The initial and boundary conditions for the coastal domains were obtained from two different CMEMS products (IBI and MED). For the hydrodynamic module, hourly barotropic currents and sea levels are consistently accommodated to the open boundaries with Chapman and Flather algorithms, whereas the variability of currents along the water column (baroclinic component), temperature and salinity are imposed from the CMEMS-IBI daily average values (or hourly data from CMEMS-MED) with clamped conditions. The initial state of the smaller domains is obtained by interpolation from the larger domain conditions.

The comparison between the HFR and modelled eastward and northward components of the surface currents (Figure A2) revealed good agreement and correlation between both datasets, both in intensity and phase, and for both spatial components. The daily oscillations correspond to the inertial period in the region (~19h) and are well reproduced by the model. Some intensifications of the currents -probably related with energetic wind events- are also well described by the model. For comparison, Figure A2 also plots the current components predicted by CMEMS-MED. For this particular period, the correlation between measured and modelled data shows an $r^2 = 0.63$, slightly larger than the correlation between CMEMS-MED data and measured values.

Regarding the currents within the bay, the fit between the modelled and measured values is shown in Figure A3. Here, the general trend of the water flow is well captured by the model, which adequately reproduces the main events, in spite of the very low energy of the system. This is a characteristic of both Ebro Delta bays, Fangar and Alfacs (Cerralbo et al., 2014, 2019) although in Fangar it is enhanced by the bay's shallowness and narrow connection with the open sea. For these verification numerical exercises, the 6-hourly ECMWF data has been used for the atmospheric forcing. For the hydro-biological simulations shown in this contribution, the 70 m grid has been used because it encompasses both the bay and part of the outer area.

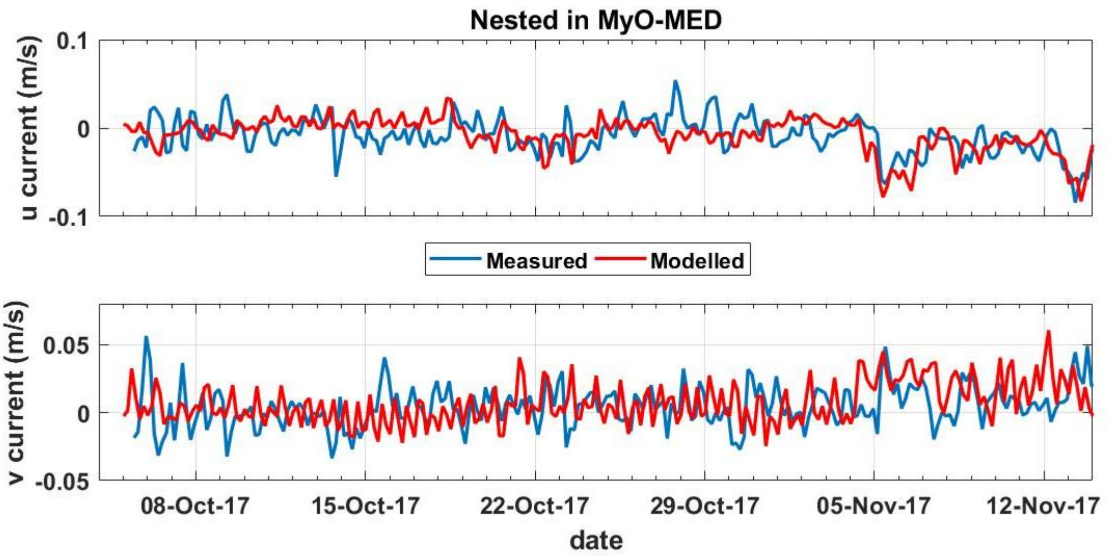

Figure A3. Surface current components U (east-west) and V (north-south) measured inside the bay (blue) and modelled by the Fangar Bay nested scheme (red) during the 2017 autumn field campaign for domain C (23 m). Correspond to boundary forcing provided by CMEMS-MED.

7. **Appendix B.** NPZD Model coupled in ROMS model.

The NPZD model follows a simple nitrogen-based scheme in order to simulate the interactions of the four variables: nutrients (N), phytoplankton (P), zooplankton (Z) and detritus (D) (Figure B1). The mathematical formulation of the internal fluxes varies in kind and complexity (see review Heinle & Slawig, 2013). This annex presents the equations used by the ROMS-NPZD model, as well as the values used for the model parameters of the numerical simulations (Table B1), which are based on the literature (i.e. Llebot et al. (2010)).

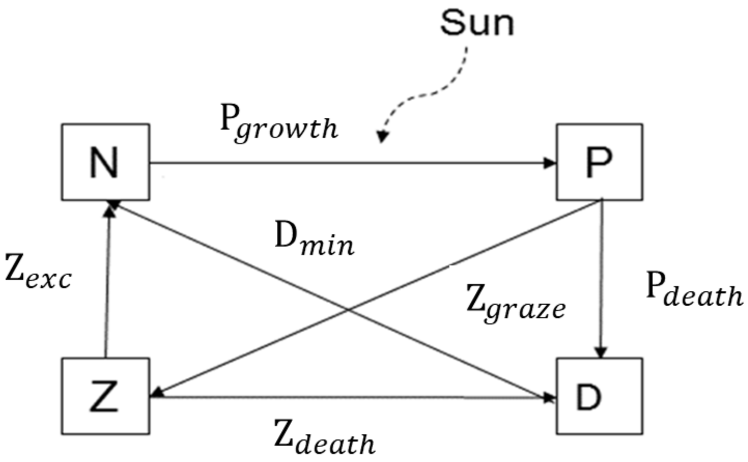

Figure B1. ROMS-NPZD model scheme including the transfer functions of the different components. N (nutrients), P (phytoplankton), Z (zooplankton) and D (detritus); P_{death} and Z_{death} is phytoplankton and zooplankton mortality respectively; P_{growth} is phytoplankton growth; Z_{exc} is zooplankton exudation; Z_{graze} is zooplankton grazing and D_{min} is remineralization.

<u>**Nutrients**</u>

$$\frac{\partial N}{\partial t} + \mathbf{u} \cdot \nabla N = \delta D + \gamma_n G Z - UP + \frac{\partial}{\partial z}\left(k_v \frac{\partial N}{\partial z}\right), \qquad \text{(B1)}$$

U = photosynthetic growth and uptake of nitrogen by phytoplankton

P = phototrophic phytoplankton
Z = herbivorous zooplankton
G = grazing on phytoplankton by zooplankton
γ_n = some proportion of the consumed phytoplankton being lost directly to the nitrate pool as a function of ‘‘sloppy feeding’’ and metabolic processes.

Phytoplankton

$$\frac{\partial P}{\partial t} + \mathbf{u} \cdot \nabla P = UP - GZ - \sigma_d P + \frac{\partial}{\partial z}\left(k_v \frac{\partial P}{\partial z}\right), \qquad \text{(B2)}$$

U = photosynthetic growth and uptake of nitrogen by phytoplankton
P = phototrophic phytoplankton
Z = herbivorous zooplankton
G = grazing on phytoplankton by zooplankton
σ_d = phytoplankton mortality

Zooplankton

$$\frac{\partial Z}{\partial t} + \mathbf{u} \cdot \nabla Z = (1 - \gamma_n)GZ - \zeta_d Z + \frac{\partial}{\partial z}\left(k_v \frac{\partial Z}{\partial z}\right), \qquad \text{(B3)}$$

Z = herbivorous zooplankton
G = grazing on phytoplankton by zooplankton
ζ_d = zooplankton mortality
γ_n = some proportion of the consumed phytoplankton being lost directly to the nitrate pool as a function of ‘‘sloppy feeding’’ and metabolic processes.

Detritus

$$\frac{\partial D}{\partial t} + \mathbf{u} \cdot \nabla D = \sigma_d P + \zeta_d Z - \delta D + w_d \frac{\partial D}{\partial z} + \frac{\partial}{\partial z}\left(k_v \frac{\partial D}{\partial z}\right), \qquad \text{(B4)}$$

Grazing

$$G = R_m\left(1 - e^{-\Lambda P}\right), \qquad \text{(B5)}$$

Uptake

$$U = \frac{V_m N}{k_N + N} \frac{\alpha I}{\sqrt{V_m^2 + \alpha^2 I^2}}. \qquad \text{(B6)}$$

Irradiance

$$I = I_0 \exp\left(k_z z + k_p \int_0^z P(z')dz'\right), \qquad \text{(B7)}$$

K_z = light extinction coefficient
k_p = self-shading coefficient

Table B1. Parameters.

Parameter name	Symbol	Value	Dimension
Light extinction coefficient	k_z	0.067	m^{-1}
Self-shading coefficient	k_p	0.08	m^2/ mmol-N
Initial slope of P-I curve	α	0.025	m^2 W^{-1}
Surface irradiance	I_o	158.075	W m^{-2}
Nitrate uptake rate	V_m	1.5	d^{-1}
Phytoplankton mortality rate (senescence)	σ_d	0.15	d^{-1}
Uptake half saturation	k_N	0.8	mmol-N · m^{-3}
Zooplankton excretion efficiency	γ_n	0.03	-
Zooplankton mortality rate	ζ_d	0.08	d^{-1}
Ivlev constant	Λ	0.06	m^3 mmol·N^{-1}
Zooplankton grazing rate	R_m	1.0	d^{-1}
Detritus remineralization rate	δ	0.1	d^{-1}
Detrital sinking rate	w_d	5.0	md^{-1}

8. Acknowledgements

The authors want to acknowledge the Ecosistema-BC Spanish research project (CTM2017-84275-R/MICINN-AEI-FEDER, UE), ECO-BAYS research project (PID2020-115924RB-I00, financed by MCIN/AEI/10.13039/501100011033) and the European Maritime and Fisheries Fund (EMFF) and the Fisheries Directorate of the Catalan Government through the project ARP029/18/00008 Carrying capacity for shellfish aquaculture in Fangar Bay. Also the CURAE project financed by Mercator Ocean International (CMEMS Service Evolution 66-SE-CALL2), and thank Jordi Cateura and Joaquim Sospedra (LIM-UPC, Barcelona, Spain) and the technical staff from IRTA for the data acquisition campaigns. As a group, we would like to thank the Secretary for Universities and Research of the Department of Economy and Knowledge of the Generalitat de Catalunya (2017SGR773).

9. Author Contributions: Conceptualization, methodology, M.F-P.B., M.G., M.E., M.M. and M.F-T.; software, M.F-P.B., M.G., M.F-T., M.M. and M.E.; validation, M.F-P.B., M.M., M.G., M.E. and M.F-T.; formal analysis, M.F-P.B.; investigation, M.F-P.B., M.G., M.E., M.M. and M.F-T.; resources, M.G., M.E, M.M. and M.F-T.; data curation, M.F-P.B., M.M. and M.F.-T.; writing—original draft preparation, M.F-P.B.; writing—review and editing, M.G., M.E., M.M., M.F.-T. and A.S-A; visualization, M.G.; supervision, M.G. and M.E.; project administration, M.E., M.G., M.F-T. and A.S.-A; funding acquisition, M.E., M.F-T and A.S-A. All authors have read and agreed to the published version of the manuscript.

10. Conflicts of Interest: The authors declare no conflict of interest. The funders had no role in the design of the study; in the collection, analyses, or interpretation of data; in the writing of the manuscript, or in the decision to publish the results.

11. References

ACA (2012) State of water bodies in Catalonia http://aca-web.gencat.cat/WDMA

Ahel, M., Barlow, R. G., and Mantoura, R. F. C. 1996. “Effect of Salinity Gradients on the Distribution of Phytoplankton Pigments in a Stratified Estuary.” *Mar. Ecol.-Prog. Ser.* 143: 289–295. https://doi.org/https://doi.org/10.3354/meps143289.

Alekseenko, E., B. Roux, A. Sukhinov, R. Kotarba, and D. Fougere. 2013. “Nonlinear Hydrodynamics in a Mediterranean Lagoon.” *Nonlinear Processes in Geophysics* 20 (2): 189–98. https://doi.org/10.5194/npg-20-189-2013.

Archetti, Genni, Sara Bernia, and Montserrat Salvà-Catarineu. 2010. “Análisis de Los Vectores Ambientales Que Afectan La Calidad Del Medio En La Bahía Del Fangar (Delta Del Ebro) Mediante Herramientas SIG.” *Revista Internacional de Ciencia y Tecnologia de La Información Geográfica* 10 (1578–5157): 252–79.

Artigas, M. L., C. Llebot, O. N. Ross, N. Z. Neszi, V. Rodellas, J. Garcia-Orellana, P. Masqué, J. Piera, M. Estrada, and E. Berdalet. 2014. “Understanding the Spatio-Temporal Variability of Phytoplankton Biomass Distribution in a Microtidal Mediterranean Estuary.” *Deep-Sea Research Part II: Topical Studies in Oceanography* 101: 180–92. https://doi.org/10.1016/j.dsr2.2014.01.006.

“Automatic Water Quality Information System, DEL EBRO, CHE-Hydrographic Confederation, Quality Alert Network, SAICA Project, 2013. Available Online: Https://Www.Saica.Co.Za/ (Accessed on 30 January 2020).” 2013.

Bolaños, R, G Jorda, J Cateura, J Lopez, J Puigdefabregas, J Gomez, and M Espino. 2009. “The XIOM: 20 Years of a Regional Coastal Observatory in the Spanish Catalan Coast.” *Journal of Marine Systems* 77 (3): 237–60. https://doi.org/10.1016/j.jmarsys.2007.12.018.

Brockmann, Carsten, Roland Doerffer, Marco Peters, Kerstin Stelzer, Sabine Embacher, and Ana Ruescas. 2016. “Evolution of the C2rcc Neural Network for Sentinel 2 and 3 for the Retrieval of Ocean Colour Products in Normal and Extreme Optically Complex Waters.”

Camp, Jordi, and M. Delgado. 1987. “Hidrogafia de Las Bahías Del Delta Del Ebro.” *Inv.Pesq.* 51 (3): 351–69.

Cerralbo, Pablo, Manel Grifoll, Arnoldo Valle-Levinson, and Manuel Espino. 2014. “Tidal Transformation and Resonance in a Short, Microtidal Mediterranean Estuary (Alfacs Bay in Ebre Delta).” *Estuarine, Coastal and Shelf Science* 145: 57–68. https://doi.org/10.1016/j.ecss.2014.04.020.

Cerralbo, P., M. Grifoll, J. Moré, A. Sairouní Afif, M. Espino, and M. Bravo. 2015. “Wind Variability in a Coastal Area (Alfacs Bay, Ebro River Delta).” *Advances in Science and Research* 12 (1): 11–21. https://doi.org/10.5194/asr-12-11-2015.

Cerralbo, Pablo, Manel Grifoll, and Manuel Espino. 2015. “Hydrodynamic Response in a Microtidal and Shallow Bay under Energetic Wind and Seiche Episodes.” *Journal of Marine Systems* 149 (Septembre): 1–13. https://doi.org/10.1016/j.jmarsys.2015.04.003.

Cerralbo, Pablo, Marta F-Pedrera Balsells, Manel Grifoll, Margarita Fernandez, Manuel Espino, Pablo Cerralbo, Marc Mestres, and Agustin Sanchez-Arcilla. 2019. “Use of a Hydrodynamic Model for the Management of the Water Renovation in a Coastal System.” *Ocean Science Discussions*, 1–20. https://doi.org/10.5194/os-2018-105.

Cloern, J. E. & Nichols, F. H. 1985. “Time Scales and Mechanisms of Estuarine Variability, a Synthesis from Studies of San Francisco Bay.” *Hydrobiologia* 29: 229–237.

D’Elia, C.F., Sanders, J.G., Boynton, W.R. 1986. “Nutrient Enrichment Studies in a Coastal Plain Estuary: Phytoplankton Growth in Large-Scale Continuous Cultures.” *Can. J. Fish. Aquat. Sci.* 43: 397–406.

Delgado, M, and Jordi Camp. 1987. “Abundancia y Distribución de Nutrientes Inorgánicos Disueltos En

Las Bahías Del Delta Del Ero.” *Inv.Pesq.* 51 (3): 427–41.

Estrada, M., Sala, M.M., van Lenning, K., Alcaraz, M., Felipe, J., Veldhuis, M.J.W. 2008. “Biological Interactions in Enclosed Plankton Communities Including Alexandrium Catenella and Copepods: Role of Phosphorus.” *J. Exp. Mar. Biol. Ecol.* 355: 1–11.

F-Pedrera Balsells, Marta, Manel Grifoll, Manuel Espino, Pablo Cerralbo, and Agustín Sánchez-Arcilla. 2020a. “Wind-Driven Hydrodynamics in the Shallow, Micro-Tidal Estuary at the Fangar Bay (Ebro Delta, NW Mediterranean Sea).” *Applied Sciences* 10 (19): 6952. https://doi.org/10.3390/app10196952.

F-Pedrera Balsells, Marta., Marc Mestres, Margarita Fernández, Pablo Cerralbo, Manuel Espino, Manel Grifoll, and Agustín Sánchez-Arcilla. 2020b. “Assessing Nature Based Solutions for Managing Coastal Bays.” *Journal of Coastal Research* 95 (sp1): 1083–87. https://doi.org/10.2112/SI95-211.1.

F-Pedrera Balsells, Marta, Manel Grifoll, Margarita Fernández-Tejedor, and Manuel Espino. 2021. “Short-Term Response of Chlorophyll a Concentration Due to Intense Wind and Freshwater Peak Episodes in Estuaries: The Case of Fangar Bay (Ebro Delta).” *Water* 13 (5): 701. https://doi.org/10.3390/w13050701.

Fasham, M. J.R., H. W. Ducklow, and S. M. McKelvie. 1990. “A Nitrogen-Based Model of Plankton Dynamics in the Oceanic Mixed Layer.” *Journal of Marine Research* 48 (3): 591–639. https://doi.org/10.1357/002224090784984678.

Fisher, T.R., Peele, E.R., Ammerman, J.W., Harding, L.W. 1992. “Nutrient Limitation of Phytoplankton in Chesapeake Bay.” *Mar. Ecol. Prog. Ser.* 82: 51–63.

Franks, Peter J.S. 2002. “NPZ Models of Plankton Dynamics: Their Construction, Coupling to Physics, and Application.” *Journal of Oceanography* 58 (2): 379–87. https://doi.org/10.1023/A:1015874028196.

Garcia, Marc A, and Antoni Ballester. 1984. “Notas Acerca de La Meteorología y La Circulación Local En La Región Del Delta Del Ebro.” *Inv.Pesq.*, 469–93.

Geyer, Natalie L., Markus Huettel, and Michael S. Wetz. 2018. “Phytoplankton Spatial Variability in the River-Dominated Estuary, Apalachicola Bay, Florida.” *Estuaries and Coasts* 41 (7): 2024–38. https://doi.org/10.1007/s12237-018-0402-y.

Geyer, W R. 1997. “Influence of Wind on Dynamics and Flushing of Shallow Estuaries.” *Estuarine, Coastal and Shelf Science* 44 (6): 713–22. https://doi.org/10.1006/ecss.1996.0140.

Gomez, F. A., Lee, S.-K., Liu, Y., Hernandez Jr., F. J., Muller-, and J. T. Karger, F. E., and Lamkin. 2018. “Seasonal Patterns in Phytoplankton Biomass across the Northern and Deep Gulf of Mexico: A Numerical Model Study.” *Biogeosciences* 15: 3561–3576. https://doi.org/https://doi.org/10.5194/bg-15-3561-2018.

Gong, X., J. Shi, H. W. Gao, and X. H. Yao. 2015. “Steady-State Solutions for Subsurface Chlorophyll Maximum in Stratified Water Columns with a Bell-Shaped Vertical Profile of Chlorophyll.” *Biogeosciences* 12 (4): 905–19. https://doi.org/10.5194/bg-12-905-2015.

Grifoll, Manel, Pablo Cerralbo, Jorge Guillén, Manuel Espino, Lars Boye Hansen, and Agustín Sánchez-Arcilla. 2019. “Characterization of Bottom Sediment Resuspension Events Observed in a Micro-Tidal Bay.” *Ocean Science* 15 (2): 307–19. https://doi.org/10.5194/os-15-307-2019.

Grifoll, Manel, Jorge Navarro, Elena Pallares, Laura Ràfols, Manuel Espino, and Ana Palomares. 2016. “Ocean-Atmosphere-Wave Characterisation of a Wind Jet (Ebro Shelf, Nw Mediterranean Sea).” *Nonlinear Processes in Geophysics* 23 (3): 143–58. https://doi.org/10.5194/npg-23-143-2016.

Guyondet Thomas, Filgueira Ramón, Pearce Christopher M., Tremblay Réjean, Comeau Luc A. 2022. “Nutrient-Loading Mitigation by Shellfish Aquaculture in Semi-Enclosed Estuaries.” *Frontiers in Marine Science* 9. https://doi.org/10.3389/fmars.2022.909926.

Haidvogel, D B, H Arango, W P Budgell, B D Cornuelle, E Curchitser, A F Shchepetkin, C R Sherwood, R P Signell, J C Warner, and J Wilkin. 2007. “Ocean Forecasting in Terrain-Following Coordinates : Formulation and Skill Assessment of the Regional Ocean Modeling System.” *Journal of Computational Physics*, 1–30. https://doi.org/10.1016/j.jcp.2007.06.016.

Hargreaves, John A. 1998. “Nitrogen Biogeochemistry of Aquaculture Ponds.” *Aquaculture* 166 (3): 181–212. https://doi.org/https://doi.org/10.1016/S0044-8486(98)00298-1.

Heinle, A., and T. Slawig. 2013. “Internal Dynamics of NPZD Type Ecosystem Models.” *Ecological Modelling* 254: 33–42. https://doi.org/10.1016/j.ecolmodel.2013.01.012.

Hickey, B. M. and Banas, N. S.: 2003. “Oceanography of the U.S. Pacific Northwest Coastal Ocean and Estuaries with Application to Coastal Ecology.” *Estuaries* 26: 1010–1031. https://doi.org/https://doi.org/10.1007/BF02803360.

Horsburgh, K. J., A. E. Hill, J. Brown, L. Fernand, R. W. Garvine, and M. M.P. Angelico. 2000. “Seasonal Evolution of the Cold Pool Gyre in the Western Irish Sea.” *Progress in Oceanography* 46 (1): 1–58. https://doi.org/10.1016/S0079-6611(99)00054-3.

Jiang, Long, Theo Gerkema, Jacco C. Kromkamp, Daphne Van Der Wal, Pedro Manuel Carrasco De La Cruz, and Karline Soetaert. 2020. “Drivers of the Spatial Phytoplankton Gradient in Estuarine-Coastal Systems: Generic Implications of a Case Study in a Dutch Tidal Bay.” *Biogeosciences* 17 (16): 4135–52. https://doi.org/10.5194/bg-17-4135-2020.

Jou, Sonia; Folch, Albert; Garcia-Orellana, Jordi; Carreño, Francisco. 2019. “Using Freely Available Satellite Thermal Infrared Data from Landsat 8 to Identify Groundwater Discharge in Coastal Areas.” *Geophysical Research Abstracts* 21: p1-1. 1p.

Llebot, Clara. 2010. “Interactions between Physical Forcing, Water Circulation and Phytoplankton Dynamics in a Microtidal Estuary.” http://digital.csic.es/handle/10261/100958?locale=es.

Llebot, Clara, Francisco J Rueda, Jordi Solé, Mireia Lara Artigas, Marta Estrada, Yvette H. Spitz, Jordi Solé, and Marta Estrada. 2014. “Hydrodynamic States in a Wind-Driven Microtidal Estuary (Alfacs Bay).” *Journal of Sea Research* 85 (3–4): 263–76. https://doi.org/10.1016/j.seares.2013.05.010.

Llebot, Clara, Jordi Solé, Maximino Delgado, Margarita Fernández-Tejedor, Jordi Camp, and Marta Estrada. 2011. “Hydrographical Forcing and Phytoplankton Variability in Two Semi-Enclosed Estuarine Bays.” *Journal of Marine Systems* 86 (3–4): 69–86. https://doi.org/10.1016/j.jmarsys.2011.01.004.

Llebot, Clara, Yvette H. Spitz, Jordi Solé, and Marta Estrada. 2010. “The Role of Inorganic Nutrients and Dissolved Organic Phosphorus in the Phytoplankton Dynamics of a Mediterranean Bay: A Modeling Study.” *Journal of Marine Systems* 83 (3–4): 192–209. https://doi.org/10.1016/j.jmarsys.2010.06.009.

Lohrenz SE, Fahnenstiel GL, Redalje DG, Lang GA, Chen X, Dagg MJ. 1997. “Variations in Primary Production of Northern Gulf of Mexico Continental Shelf Waters Linked to Nutrient Inputs from the Mississippi River.” *Marine Ecology Progress Series* 155: 45–54. https://www.int-res.com/abstracts/meps/v155/p45-54/.

Lorente P., Piedracoba S., Soto-Navarro J., Álvarez-Fanjul E. 2015. “Evaluating the Urface Circulation in the Ebro Delta (Northeastern Spain) with Quality-Controlled High-Frequency Radar Measurements.” *Ocean Science* 11 (6): 921-935.

Madariaga, Iosu de. 1995. “Photosynthetic Characteristics of Phytoplankton During the Development of a Summer Bloom in the Urdaibai Estuary, Bay of Biscay.” *Estuarine, Coastal and Shelf Science* 40 (5): 559–75. https://doi.org/10.1006/ecss.1995.0038.

Martin, M. A., Fram, J. P., and Stacey, M. T. 2007. “Seasonal Chlorophyll a Fluxes between the Coastal Pacific Ocean and San Francisco Bay.” *Mar. Ecol.-Prog. Ser.* 337: 51–61. https://doi.org/https://doi.org/10.3354/meps337051.

Muñoz, I. 1990. “Limnología de La Part Baixa Del Riu Ebre i Els Canals de Reg: Els Factors Fisico-Quimics, El Fitoplancton i Els Macroinvertebrats Bentonics. Tesis Para La Postulación Al Grado de Doctor. Departamento de Ecología. Facultad.” Facultad de Biología. Universidad de Barcelona.

Oschlies, A. 2001. “Model-Derived Estimates of New Production: New Results Point towards Lower Values.” *Deep-Sea Research Part II: Topical Studies in Oceanography* 48 (10): 2173–97. https://doi.org/10.1016/S0967-0645(00)00184-3.

Perez, Marta, Camp, Jordi. 1986. “Distribución Espacial y Biomasa de Las Fanerógamas Marinas de Las Bahías Del Delta Del Ebro” 50: 519–30.

Pontee, N, Narayan, S, Beck MW and Hosking AH. 2016. “Nature-Based Solutions: Lessons from around the World.” *Proceedings of the Institution of Civil Engineers* 169(1): 29–36.

Powell, Thomas M, Craig V W Lewis, Enrique N Curchitser, Dale B Haidvogel, Albert J Hermann, and Elizabeth L Dobbins. 2006. “Results from a Three-Dimensional, Nested Biological-Physical Model of the California Current System and Comparisons with Statistics from Satellite Imagery.” *Journal of Geophysical Research: Oceans* 111 (7): 1–14. https://doi.org/10.1029/2004JC002506.

Quijano-Scheggia, Sonia, Esther Garcés, Eva Flo, Margarita Fernandez-Tejedor, Jorge Diogène, and Jordi Camp. 2008. “Bloom Dynamics of the Genus Pseudo-Nitzschia (Bacillariophyceae) in Two Coastal Bays (NW Mediterranean Sea).” *Scientia Marina* 72 (3): 577–90.

Ràfols, Laura, Manel Grifoll, Gabriel Jordà, Manuel Espino, Abdel Sairouní, and Manel Bravo. 2017. “Shelf Circulation Induced by an Orographic Wind Jet.” *Journal of Geophysical Research: Oceans* 122 (10): 8225–45. https://doi.org/10.1002/2017JC012773.

Ramón, M, M Fernández, and E Galimany. 2007. “Development of Mussel (Mytilus Galloprovincialis) Seed from Two Different Origins in a Semi-Enclosed Mediterranean Bay (N.E. Spain).” *Aquaculture* 264 (1–4): 148–59. https://doi.org/10.1016/j.aquaculture.2006.11.014.

Reguera, B., Bravo, I., Mariño, J., Campos, M.J., Fraga, S., Carbonell, A. 1993. “Trends in the Occurrence of Dinophysis Spp. in Galician Coastal Waters.” *Toxic Phytoplankton Blooms in the Sea. Elsevier*, 559–564.

Rico, Jorge Eduardo Cruz. 2015. “Análisis de La Variabilidad de La Clorofila En La Bahía de Todos Santos a Través de Un Modelo Numérico Físico-Biológico.” Centro de Investigación Científica y de Educación Superior de Ensenada, Baja California.

Shchepetkin, Alexander F., and James C. McWilliams. 2005. “The Regional Oceanic Modeling System (ROMS): A Split-Explicit, Free-Surface, Topography-Following-Coordinate Oceanic Model.” *Ocean Modelling* 9 (4): 347–404. https://doi.org/10.1016/j.ocemod.2004.08.002.

Simpson, J. H., and D. Bowers. 1981. “Models of Stratification and Frontal Movement in Shelf Seas.” *Deep Sea Research Part A. Oceanographic Research Papers* 28 (7): 727–38. https://doi.org/10.1016/0198-0149(81)90132-1.

Soetaert, K., Middelburg, J. J., Heip, C., Meire, P., Van Damme, and T. S., and Maris. 2006. “Long-Term Change in Dissolved Inorganic Nutrients in the Heterotrophic Scheldt Estuary (Belgium, The Netherlands).” *Limnol. Oceanogr.* 51: 409–423. https://doi.org/https://doi.org/10.4319/lo.2006.51.1_part_2.0409.

Soriano-González, Jesús, Eduard Angelats, Margarita Fernández-Tejedor, Jorge Diogene, and Carles Alcaraz. 2019. “First Results of Phytoplankton Spatial Dynamics in Two NW-Mediterranean Bays from Chlorophyll-A Estimates Using Sentinel 2: Potential Implications for Aquaculture.” *Remote Sensing* 11 (15). https://doi.org/10.3390/rs11151756.

Srichandan, S., Kim, J. Y., Kumar, A., Mishra, D. R., Bhadury, and G. P., Muduli, P. R., Pattnaik, A. K., and Rastogi. 2015. “Interannual and Cyclone-Driven Variability in Phytoplankton Communities of a Tropical Coastal Lagoon.” *Mar. Pollut. Bull.* 101: 39–52. https://doi.org/https://doi.org/10.1016/j.marpolbul.2015.11.030.

Stow, C. A., Jolliff, J., McGillicuddy Jr., D. J., Doney, S. C., Allen, J. I., Friedrichs, M. A., and P. M., Rose, K. A., y Walhead. 2009. “Skill Assessment for Coupled Biological/Physical Models of Marine Systems.” *Journal of Marine Systems* 76: 4–15.

Wan, Yongshan, Chelsea Qiu, Peter Doering, Mayra Ashton, Detong Sun, and Teresa Coley. 2013. “Modeling Residence Time with a Three-Dimensional Hydrodynamic Model: Linkage with Chlorophyll a in a Subtropical Estuary.” *Ecological Modelling* 268: 93–102. https://doi.org/10.1016/j.ecolmodel.2013.08.008.

Warner, J. C., Geyer, W. R., and Lerczak, J A.: 2005. “Numerical Modeling of an Estuary: A Comprehensive Skill Assessment.” *Journal of Geophysical Research: Oceans* 110 (C05001).

https://doi.org/10.1029/2004JC002691,.

Weitzman, Jenny, and Ramón Filgueira. 2020. “The Evolution and Application of Carrying Capacity in Aquaculture: Towards a Research Agenda.” *Reviews in Aquaculture* 12 (3): 1297–1322. https://doi.org/https://doi.org/10.1111/raq.12383.

Xie, Xiaohui, and Ming Li. 2018. “Effects of Wind Straining on Estuarine Stratification: A Combined Observational and Modeling Study.” *Journal of Geophysical Research: Oceans* 123 (4): 2363–80. https://doi.org/10.1002/2017JC013470.

Yu, Liuqian, and Jianping Gan. 2021. “Mitigation of Eutrophication and Hypoxia through Oyster Aquaculture: An Ecosystem Model Evaluation off the Pearl River Estuary.” *Environmental Science & Technology* 55 (8): 5506–14. https://doi.org/10.1021/acs.est.0c06616.